NSRRC-J05087 (2016)

PCCP

PAPER

View Article Online
View Journal | View Issue

Cite this: *Phys. Chem. Chem. Phys.*, 2016, 18, 3179

Intrinsic coordination for revealing local structural changes in protein folding–unfolding†

Ying-Jen Shiu,[ab] Michitoshi Hayashi,*[c] Orion Shih,[a] Charlene Su,[b] Min-Yeh Tsai,[d] Yi-Qi Yeh,[a] Chun-Jen Su,[a] Yu-Shan Huang,[a] Sheng-Hsien Lin[bd] and U-Ser Jeng*[ae]

Received 17th October 2015,
Accepted 22nd December 2015

DOI: 10.1039/c5cp06309d

www.rsc.org/pccp

With a deformed object of a rigid rod inside, the local dislocations may be tracked relatively easily with respect to the internal rigid rod. We apply this concept on protein folding–unfolding to track the internal structural changes of an unfolded protein in solution. Proposed here is a protein internal coordination based on the major axis X of an ellipsoidal protein and the stable intrinsic transition dipole moment μ of the protein during unfolding. In this methodology, small-angle X-ray scattering (SAXS) is used to provide the protein global morphologies in the native and unfolded states. Furthermore, time-resolved fluorescence anisotropy (TRFA) provides the relative orientation between X and μ of Trp59 of the model protein cytochrome *c*. Hence observed in the protein unfolding with denaturants, acid, urea, or GuHCl, is the elongation of the native protein conformation along a reoriented protein major axis; accompanied are the different extents of relocations of the terminal α helices and loop structures of the protein in the corresponding unfolding.

1. Introduction

Proteins need specific conformations for their biological functions *in vivo*. In particular, conformational changes of protein folding are of great importance in biomedical science, as accumulation of partially-unfolded or mis-folded proteins may lead to misfunction or aggregation that eventually results in fatal diseases such as Alzheimer's and Creutzfeldt-Jakob diseases.[1–5] As a result, abundant experimental and theoretical efforts have focused on the elucidation of protein folding–unfolding processes and demonstrated that a functional, stable protein structure greatly demands collective intramolecular peptide (amide) hydrogen bonding, charge interactions, as well as hydrogen bonding with the surrounding water molecules in solution.[6–12] Consequently, environmental factors, such as denaturants, temperature, and solution ionic strength, can modify the intra- and inter-hydrogen bonding network of proteins, leading to activation or suppression of a particular protein function.[13–20] The detailed protein folding–unfolding process may reveal crucial hints on how a protein functional structure is established or disrupted *via* the interplay between internal and external interactions.

Pioneer studies showed that folding kinetics and local structural changes of protein subdomains could be revealed based on optical approaches. For instance, the T-jump technique with nanosecond laser and oriented circular dichroism (CD) were applied to observe the early stage of protein folding events of the secondary structure;[21,22] the spectroscopy of second harmonic generation (SHG) and sum-frequency generation (SFG) were used to reveal orientations of biomacromolecules at interfaces.[23–26] To investigate global structural changes of proteins *via* monitoring local structural dynamics, ultrafast two-dimensional infrared (2D-IR) vibrational echo spectroscopy was performed to reveal a time-resolved protein unfolding evolution through the changes in the labelled vibrational frequency.[27,28] Previously, we used a combination of structural tools of small-angle X-ray scattering (SAXS), circular dichroism (CD), and UV-Vis absorption to reveal correlations between the global and local structural changes of a model protein cytochrome *c* (cyt *c*) unfolding in a single or compounded denaturing environment.[29–31] These studies suggested that collective local structural changes would contribute altogether to the global structural change. Despite these successes, characterization of the local structural changes with respect to the global morphology in protein folding–unfolding is still difficult to track during the processes without a convenient coordination. Such information provides critical insights into

[a] *National Synchrotron Radiation Research Center, Hsinchu 30076, Taiwan. E-mail: usjeng@nsrrc.org.tw*
[b] *Institute of Atomic and Molecular Sciences, Academia Sinica, P. O. Box 23-166, Taipei 106, Taiwan*
[c] *Center for Condensed Matter Sciences, National Taiwan University, Taipei 106, Taiwan. E-mail: atmyh@ntu.edu.tw*
[d] *Department of Applied Chemistry, National Chiao Tung University, Hsinchu 300, Taiwan*
[e] *Department of Chemical Engineering, National Tsing Hua University, Hsinchu 30013, Taiwan*

† Electronic supplementary information (ESI) available: Supporting materials, equation details, two figures and eight tables. See DOI: 10.1039/c5cp06309d

the protein unfolding mechanism beyond cause-and-effect understanding.

In this work, we propose a possible intrinsic internal coordination established from the major axis X of an ellipsoidal protein and the stable intrinsic transition dipole moment $\boldsymbol{\mu}$ of the protein during unfolding, to track unfolding processes of a model protein cyt *c*. This intrinsic coordination provides a comprehensive presentation of the protein unfolding orientation with respect to the native protein structure. Previous studies[29–31] have demonstrated that SAXS can provide decent protein global envelopes, hence the shape anisotropy of the protein. With the shape information, time-resolved fluorescence anisotropy (TRFA) can further reveal the relative orientation of the major axis of the protein morphology with respect to the transition dipole moments of Trp59 of cyt *c*.[32] On the basis of the internal coordination with $\boldsymbol{\mu}$ and X, we observe the unfolding pathways of cytochrome *c* denatured by urea, GuHCl, or acid, and suggest trends of relocation of the local structures in the corresponding unfolding processes. The proposed TRFA–SAXS approach shares an underlying principle of probing the site-specific orientation of biomolecules with the methodologies of site-specific SFG and 2D-IR,[26] and is limited to proteins with single Trp residue. Nevertheless, the approach may be extended to proteins with multiple Trp residues provided Trp-derivative probes can be developed to emit at a different wavelength.[27,28] Alternatively, attaching chromophores to selected sites of a protein may further broaden the application of these methodologies.

2. Experimental details

2.1 Sample preparation

Horse heart cytochrome *c* (cyt *c*) in an oxidized form (M_w = 12 384 Da) was purchased from Sigma Chemicals, and used without further purification. Aqueous solutions of cyt *c*, 20 μM or 0.4–0.8 mM, were prepared, respectively, for TRFA or SAXS measurements. The buffer solution contained 7 mM potassium phosphate and 7 to 21 mM KCl for adjusting the solution ionic strength. Denatured cyt *c* solutions were prepared using 4.0 M guanidinium chloride (GuHCl) at pH = 6.3, 8.0 M urea at pH = 6.6, or acid at pH = 1.9. The protein morphology in solution was shown to be insensitive to pH values between 6 and 7 previously.[31]

2.2 SAXS measurements and data analysis

SAXS data were collected at the NSRRC SWAXS Beamline 23A, Hsinchu, Taiwan.[33] Sample solutions were, respectively, loaded into thermostated cells, 40 μl each, at 15 °C. With 15 keV X-rays (wavelength λ = 0.827 Å) and a sample-to-detector distance of 2.5 m, the wavevector transfer q is defined by $4\pi\lambda^{-1}\sin\Theta$ with scattering angle 2Θ. Data were collected with 1 frame per 60 s for 5 successive frames using a Pilatus 1M-F area detector; frame data for identical profiles (*i.e.* no sign of radiation damage) were combined for improved data statistics. Sample solution scattering was subtracted from the corresponding buffer solution scattering collected under identical experimental conditions.[33] Analysis of SAXS data for protein envelopes in solution followed the method reported previously,[30,31,34] using monodispersed ellipsoids of semi-major and semi-minor axes c and a, and the aspect ratio $\rho = c/a$. The approximated ellipsoid model fitting result was examined further with the protein envelopes obtained, with the same set of SAXS data, using the simulation package adopted from the EMBL Biological Small Angle Scattering Group.[35] Three-dimensional shape reconstructions were also generated *via* GASBOR,[35] and 20 models were generated *via* independent runs for each set of SAXS data. When the average normalized spatial discrepancy (NSD) for the 20 models was smaller than one, the set was considered a single cluster, and the model with the lowest NSD was considered as the representative model.

2.3 TRFA measurements and analysis

TRFA measurements were performed using a time-correlated single photon counting instrument (Fluo Time 200, PicoQuant Inc.), with a response function of 26 ps and a time resolution of 0.8 ps. The sample solutions, filled in a quartz cuvette with 2 mm light path, were excited by a 270 nm ultrafast laser. The excitation light was generated by the third harmonic generator (TP-1B, Femtochrome Research Inc.), which was pumped by a Ti:sapphire laser (Mira 900, Coherent Inc.) at 100 fs pulse width and 76 MHz repetition rate. Emission from the sample solution was collected in the direction perpendicular or parallel to the laser excitation, and analyzed at 350 nm especially for Trp59 emission of cyt *c*. TRFA data analysis was conducted as the following: (1) a rigid and axial symmetric rotor was established for cyt *c*, using the aspect ratio of the protein morphology provided by the corresponding SAXS result and (2) the Euler angles were determined to build up the relative orientations between the two frames that were designated for the protein morphology and emission transition dipole moments of the fluorophore Trp59 of cyt *c*.[32] For a linear system with negligible instrument response function, the time-dependent anisotropy equation $r(t)$ could be approximated by

$$r(t) = (I_{\parallel}(t) - \sigma\cdot I_{\perp}(t))/(I_{\parallel}(t) + 2\sigma\cdot I_{\perp}(t)) \quad (1)$$

with the two polarized emissions $I_{\parallel}(t)$ and $I_{\perp}(t)$, respectively, being parallel and perpendicular to the polarization of the incident light; σ is a scaling factor for instrument response efficiency to the polarized emission.[36–40] On the basis of a previously proposed, randomly oriented prolate rotor of TRFA,[41] $r(t)$ can be modeled by an axial symmetric rotor with decreased degrees of freedom and the two rotational diffusion constants $D_{\parallel}$ and $D_{\perp}$ as

$$\begin{aligned} r(t) = 6/5\cdot\{&(A\cdot B)\exp(-(D_{\parallel} + 5D_{\perp})t) \\ &+ 1/4\cdot(2A^2 + B^2 + C^2 - 2/3)\exp(-6D_{\perp}t) \\ &+ 1/4\cdot(B^2 - C^2)\exp(-(4D_{\parallel} + 2D_{\perp})t)\} \end{aligned} \quad (2)$$

where $A = (\cos\theta\cos\gamma - \sin\theta\cos\chi\sin\gamma)\cos\theta$, $B = (\sin\theta\cos\gamma + \cos\theta\cos\chi\sin\gamma)\sin\theta$, and $C = \sin\theta\sin\chi\sin\gamma$ (*cf.* Fig. 1). Moreover, the ratio of rotational diffusion time constants $D_{\perp}/D_{\parallel} = ((2\rho^2 - 1)S - \rho)/((\rho - S)(\rho^2 + 1))$, with $S = \ln\left(\rho + \sqrt{\rho^2 - 1}\right)\Big/\sqrt{\rho^2 - 1}$, is associated with the aspect

This journal is © the Owner Societies 2016

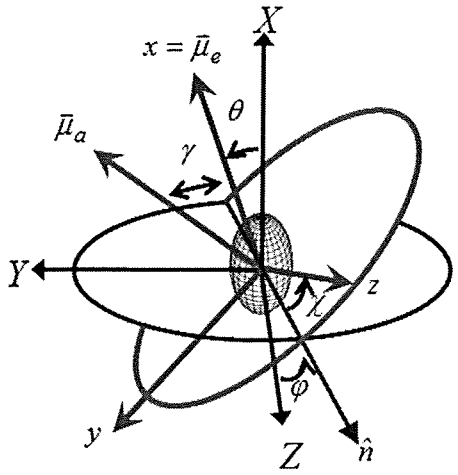

Fig. 1 Relative orientations (φ, θ, χ) between the x–y–z frame for the intrinsic transition dipole moments and the X–Y–Z frame for the protein morphology with the major axis of the ellipsoidal protein aligned along the X-axis. The black circle is in the YZ plane, the red circle is in the yz plane, and the intersection of the two circles is given by the vector $\hat{n}$. The emission transition dipole moment $\vec{\mu}_e$ is oriented along the x-axis, forming an included angle γ with the absorption transition dipole moment $\vec{\mu}_a$ (the blue arrow) on the xy plane.

ratio ρ of the protein morphology according to the Navier–Stokes equation.[41] Assuming a randomly oriented prolate rotor of protein cyt c, we can extract the angles $\{\theta, \chi, \gamma\}$ associated with the protein internal coordination *via* integrating TRFA and SAXS. Fig. 1 illustrates the relative orientation, in terms of the deduced Euler angles (φ, θ, χ), for the two frames: x–y–z for the intrinsic transition dipole moments and X–Y–Z for the protein morphology; where θ is the angle between the major axis of the rotor and the emission transition dipole moment. The term γ represents the angle between emission and absorption transition dipole moments. The frame (x, y, z) is spanned by the emission and the absorption transition dipole moments, $\vec{\mu}_e$ and $\vec{\mu}_a$, of Trp59, together with the normal vector $\vec{N}$ of the $\vec{\mu}_e \times \vec{\mu}_a$ plane. Thus, the x axis is given by $\vec{\mu}_e$, the y axis by $\vec{\mu}_a'$, and the z axis by $\vec{N}$, the detailed definitions are given in the ESI† (S1–S3).

The major axis $\vec{X}_I$ of a protein in the (X, Y, Z) frame is mapped onto the native protein coordinate adopted directly from the crystalline structure (code 1HRC),[32] and it is transformed into $\vec{X}_I'$ *via*

$$\vec{X}_I' = T_I \cdot R_I \cdot \vec{X}_I - \vec{O} \text{ with } \vec{X}_I = \begin{pmatrix} 1 \\ 0 \\ 0 \end{pmatrix}. \quad (3)$$

The R-matrix correlates the unfolded morphologies and Trp59, with the subscript I representing N or U for the native or unfolded protein; the T-matrix is associated with the absorption and emission transition dipole moments $\vec{\mu}_a$ and $\vec{\mu}_e$ of Trp59. For instance, $\vec{X}_U'$ denotes the major axis of the unfolded cyt c structure modelled with an ellipsoidal envelope; while $\vec{X}_N'$ indicates that of the native cyt c structure. The coordinate origin $\vec{O}$ is allocated to the center of mass of the native cyt c. Here, we have ignored the effects of the internal rotation of the fluorophore Trp59.

3. Results and discussion

3.1 SAXS and global morphology

Shown in Fig. 2 are the SAXS results for the native cyt c and the protein unfolded by urea, GuHCl, and acid, respectively. These SAXS data deviate significantly from the power-law scattering $I(q) \propto q^{-2}$ for random coils (Fig. 2), implying that unfolded cyt c under these denaturing conditions still holds a residual 3-D structure.[42] Using the monodispersed ellipsoid model and as discussed previously,[30,31] we fitted all the SAXS data (Fig. 2) reasonably well, using the semi-axis values of a and c.

The hence deduced aspect ratios ρ, summarized in Table 1, drastically increased from 1.3 for the native protein to 6.0, 6.6, and 3.3, respectively, for the protein unfolded by 8 M urea, 4 M GuHCl, and acid (pH = 1.9). The result indicates substantially

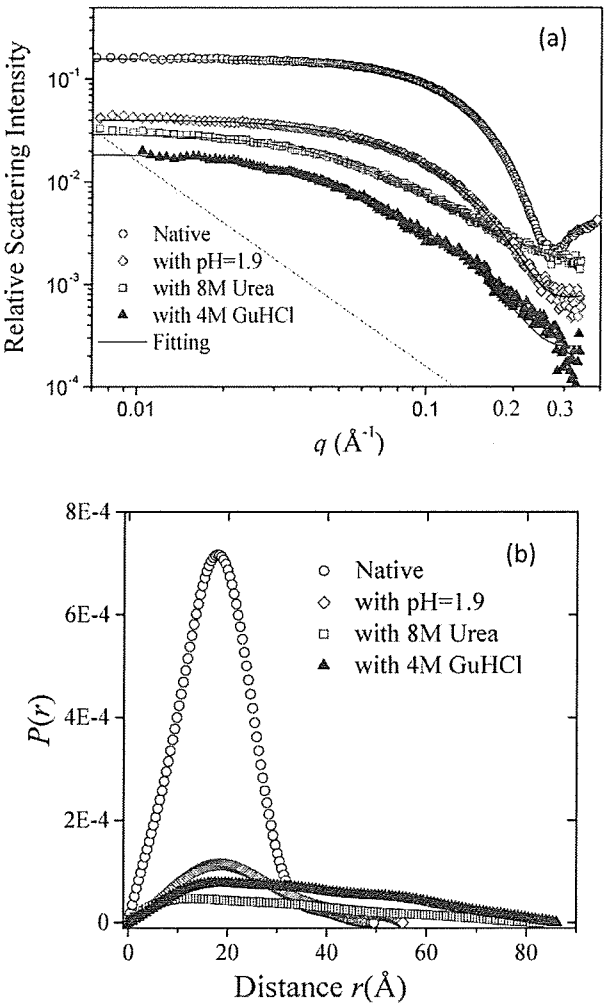

Fig. 2 (a) SAXS data for the native cyt c and that unfolded with 4 M GuHCl, 8 M urea, and acid (pH = 1.9), respectively. The data are fitted (solid curves) using simplified ellipsoidal shapes with major and minor axes a and c. The dotted line shows the power-law scattering $I(q) \propto q^{-2}$. (b) Corresponding $P(r)$ functions from the SAXS data.

Table 1 The fitted Euler angles θ, χ and γ (*cf.* Fig. 1) and the two diffusion rotational time constants ($D_{\parallel}$ and $D_{\perp}$) of cyt *c* in the native or unfolded state at pH = 1.9, 8 M urea, or 4 M GuHCl, with φ = 0. The aspect ratios ρ = *c*/*a* are deduced from the ellipsoid model fitting results with the corresponding SAXS data (*cf.* Fig. 2)

	Native	Acid pH 1.9	8 M Urea	4 M GuHCl
θ (°)	77.0 ± 44.2	78.1 ± 1.3	53.7 ± 0.8	54.4 ± 0.3
χ (°)	56.6 ± 15.6	57.0 ± 0.4	61.6 ± 11.4	46.4 ± 1.9
γ (°)	45.5 ± 0.9	41.9 ± 0.2	47.7 ± 0.06	42.9 ± 0.2
ρ	1.27 ± 0.08	3.30 ± 0.04	6.0 ± 0.1	6.6 ± 0.1
$D_{\perp}/D_{\parallel}$	0.84	0.28	0.116	0.099
$D_{\parallel}$ (ns^{-1})	0.26 ± 0.01	0.38 ± 0.3	0.23 ± 0.14	0.25 ± 0.02

Table 2 Representative models (with surrounding water molecules) obtained from the SAXS data fitting using GASBOR. Also shown are the corresponding D_{max}, average aspect ratios measured from the fitted envelopes and fitting quality index χ^2

	Native	pH 1.9	8 M urea	4 M GuHCl
	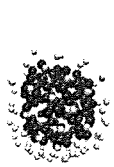			
χ^2	1.3	1.2	~1.0	~1.0
D_{max} (Å)	50	55	83	86
ρ	1.3 ± 0.1	3.8 ± 0.6	6.1 ± 1.3	6.3 ± 1.8

elongated protein morphologies for the unfolded protein, suggesting a preferred unfolding direction along the major axis *c* of the protein.

The pair correlation functions $P(r)$ (Fig. 2b) Fourier transformed from the SAXS data were also analyzed using the GASBOR model, based on a chain-like ensemble of dummy residues for *ab initio* reconstruction of the protein envelopes.[35] The ensemble conformations (detailed in Table S1 of the ESI†) hence fitted suggest relatively converged shapes of ellipsoid proximity for the unfolded cyt *c*. From the ensembles, we have obtained consistent aspect ratios, within differences less than 15% from that extracted using the ellipsoid model (Table 2). Such difference in the aspect ratio is found to only marginally change (<10%) the values of TFRA-fitted parameters as detailed below. The representative protein envelopes extracted from the $P(r)$ functions and the corresponding D_{max} values (the maximum distance of the protein) are summarized in Table 2.[35]

3.2 TRFA results and local structures

Fig. 3a–c display the measured time-resolved TRFA profiles of the cyt *c* unfolded in the denaturing environments studied (4 M GuHCl, urea 8 M, and acid pH 1.9). These profiles were derived from the fluorescence decay curves measured with parallel and perpendicular emission polarization (insets of Fig. 3a–c), and analyzed using a prolate rotor comprising three exponential decays, as illustrated in eqn (2). With the SAXS input of the aspect ratios being 1.3, 3.3, 6.0, and 6.6, respectively, for the

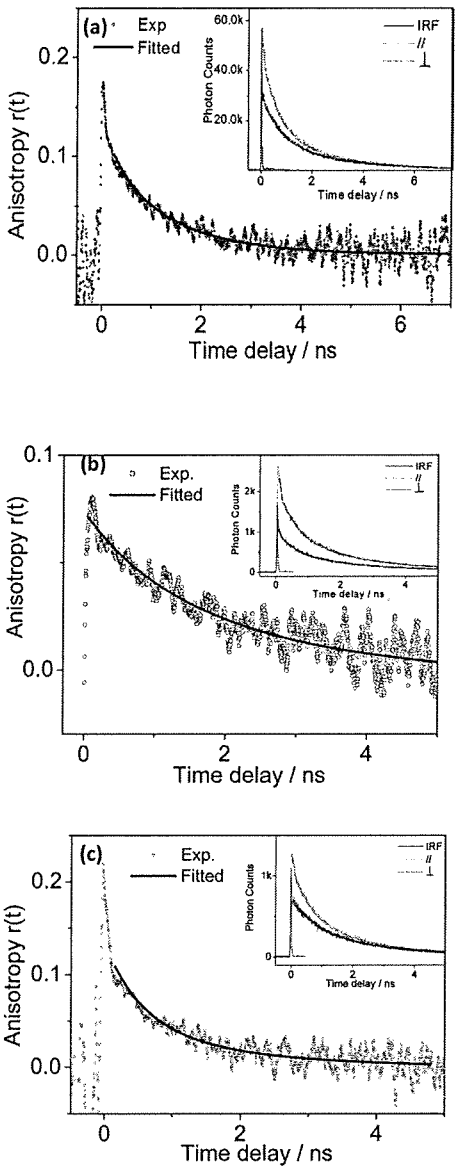

Fig. 3 Representative anisotropy profile measured for cyt *c* unfolded with (a) 4 M GuHCl at pH 6.3; (b) 8 M urea at pH 6.6; and (c) acid at pH 1.9. Insets display the corresponding anisotropic fluorescence decay profiles measured, respectively, with fluorescence polarization being perpendicular and parallel to the excitation polarization.

native protein and the protein unfolded by acid, urea, and GuHCl, we could fit reasonably well all the TRFA profiles (shown in Fig. 3) with φ = 0; the correspondingly fitted $D_{\perp}/D_{\parallel}$ ratios, $D_{\parallel}$ together with the orientation angle values for θ, χ and γ, are listed in Table 1.

The TRFA profiles were best-fitted with three individual decay time constants spread in the range of 0.3 ns^{-1} to 1.8 ns^{-1}; from the time constants, values of $D_{\parallel}$ and $D_{\perp}$ were derived. The orientation angle changes shown in Table 1 suggest that these protein unfolding processes can be best characterized by the major changes in the angle θ between the protein major axis (*X*-axis) and the transition dipole moment $\vec{\mu}_e$ (*x*-axis). For the native protein, θ is found to be 77°;

This journal is © the Owner Societies 2016

whereas in the case of urea or GuHCl unfolding θ drops significantly to *ca.* 54° (Table 1). This observation suggests significant relocations of the local structures during the unfolding process. Whereas the relatively small change in θ for the acid unfolding implies that the protein is elongated along the major axis of the native protein without much disturbance of Trp59. This would imply a different acid unfolding pathway with relatively less relocations of the local structures. In contrast, negligible changes were observed in the angle γ in all the three denaturing conditions, implying relatively stable electronic states of $\vec{\mu}_a$ and $\vec{\mu}_e$ in the unfolding environments. Such results support our proposed methodology that the stable transition dipole moments may be used as an internal coordination for the projection of relative structural changes in the protein unfolding.

We note that a previous TRFA study already revealed an internal conversion (IC) time constant less than 100 fs for free tryptophans in solution,[43] namely, the local process of IC could be accomplished efficiently before large protein morphology changes take place. Therefore, we neglected the IC effect in the analysis of the anisotropy profile. Two additional small effects regarding the energy transfer between the fluorophores (Trp59) and the internal rotation of the fluorophore were also neglected, respectively, owing to the low protein concentration used and the rigid-body rotor assumed. The latter assumption is based on the fact that the Trp59, being next to the 60's α-helix in the amino acid sequence and nearby the heme, is buried in the center of the protein. Because of the steric hindrance and the hydrogen bonds, the buried Trp59 is rigid in native cyt *c* and therefore the internal rotation can be ignored.[43] We have measured and compared the time-resolved fluorescence decay profiles of free tryptophans and the Trp59 of the unfolded protein in the same denaturing environments; the result (Fig. S2, ESI†) suggests that the hence unfolded cyt *c* conformations still could cover the Trp59 reasonably well, hence hindering largely the free rotation of the indole ring of Trp59 of the protein in the unfolding environment.

We have also examined the SAXS model effect, ellipsoid *vs.* GASBOR model, on TRFA analysis. The not-large differences (<15%) in the averaged aspect ratios obtained from the two methods for all cases studied marginally change the values (<10%) of the TRFA-deduced parameters, as detailed in Tables S2 and S3 (ESI†). The result suggests that although the ellipsoid shape adopted is not an ideal shape for the unfolded protein it may be acceptable as a convenient step in simplifying the present approach.

3.3 Quantum chemistry model calculations for Trp59

To address the local structure $\vec{\mu}_a$ and $\vec{\mu}_e$ of Trp59 in the protein, we have conducted quantum chemistry model calculations based on the cyt *c* crystalline structure (code 1HRC). In the model calculation, the corresponding hydrogen atoms were added to the crystal structure.[32] We note that the transition dipole moments of Trp59 involve mainly the π–π* transitions in the indole ring of the tryptophan. Conventionally, this N–H bonding is co-planed with the indole ring (0° for the N–H tilt angle to the indole ring) for a minimized potential energy surface of the tryptophan without solvent effects.[44] Nevertheless, to match the γ angle observed with our TRFA result (Table 1), we have to use a most consistent N–H tilt angle of $-45 \pm 1.5°$, leading to a dihedral angle C_α–C_β of $177 \pm 1.5°$ (N–H and C_α–C_β on the opposite sides of the indole ring). According to a previous report,[44] non-coplanar N–H could occur due to the hydrogen bond donation to the indole ring. Most likely, the unusual tilt angle of N–H in our calculation could be a transit tryptophan structure excited during the TRFA measurements, during which, the non-coplanar N–H bonding might be provoked by collective effects of solvent and the neighborhood residues, as detailed in the ESI† (S6–S8). Fig. 4 shows the hence determined tryptophan structure with $\vec{\mu}_a$ and $\vec{\mu}_e$ for the native protein. The Trp59 structures calculated with the corresponding γ angles observed in the three denaturants show only marginal differences (*cf.* Table 1), suggesting that the structure is sufficiently stable under these unfolding conditions. Therefore, using the transition dipole moments of Trp59 as reference coordinate vectors for the folding–unfolding process (Table 1) should be objective.

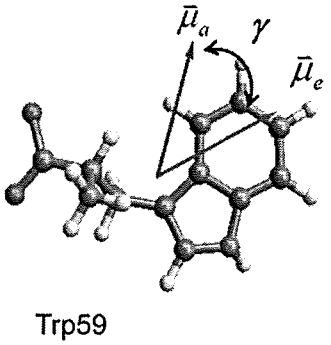

Fig. 4 The structure of Trp59 of cyt *c* reconstructed based on the quantum chemistry calculations and the TRFA results. The blue and red arrows indicate the absorption and emission transition dipole moments $\vec{\mu}_a$ and $\vec{\mu}_e$. The intercept of the two vectors is allocated to the center of mass of the tryptophan.

3.4 Protein internal coordination

Representatively illustrated in Fig. 5 are the deduced major axis $\vec{X}_U'$ of the unfolded protein by urea superimposed onto the native protein structure of cyt *c*. Some representative parts of the local structure of the native protein are given by vectors: the C-terminal α-helix vector $\vec{\alpha}_C$, N-terminal α-helix vector $\vec{\alpha}_N$, and 60's α-helix vector $\vec{\alpha}_{60}$. The protein intrinsic vectors such as the heme-ligand vectors ($\vec{v}_{Fe-Trp59}$ and $\vec{v}_{Fe-S(Met80)}$) and the total dipole moment $\vec{v}_D$ are also given. The vector directions of the α-helices are defined to be along the increase of the residue sequence, (detailed in S9–S11, ESI†). The corresponding included angles of these vectors with $\vec{X}_I'$ are deduced from the crystal structure and summarized in Table 3. Also shown in Table 3 are the included angles of these characteristic protein vectors with the major axis $\vec{X}_U'$ of the unfolded protein of an ellipsoidal envelope. We emphasize that the hence resolved evolution of the protein major axis (from $\vec{X}_N'$ to $\vec{X}_U'$) with respect to $\vec{\mu}_e$ provides insights/projections on how the protein local structures would relocate in the unfolding process. Therefore, the major axis $\vec{X}_U'$ of the

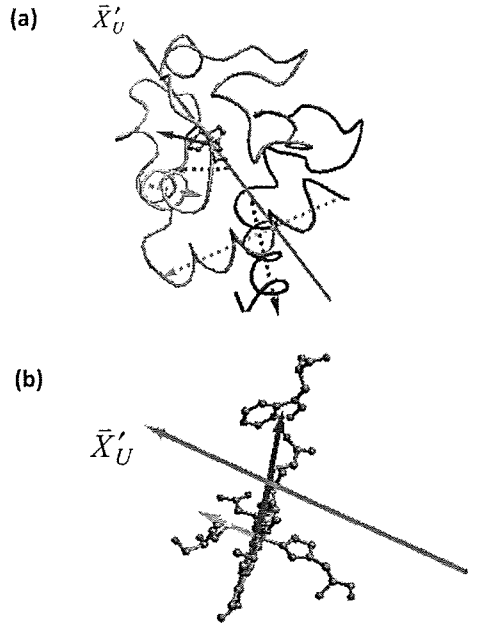

Fig. 5 (a) Extracted urea-unfolded protein major axis $\vec{X}_U'$ (gray arrow) overlapping the native protein conformation (wireframe) with the intrinsic emission transition dipole moment $\vec{\mu}_e$ (red arrow) of Trp59 and the helical vectors. The orange, purple, green, and brown dashed arrows indicate the C-terminal α-helical vector, N-terminal α-helical vector, 60's α-helical vector, and the total dipole moment of the native cyt *c*, respectively. (b) Relationship between the protein intrinsic vectors of Fe–Trp59 (center blue arrow) and Fe–S(Met80) (short pink arrow below) and the extracted unfolded protein major axis $\vec{X}_U'$ for the unfolded protein.

Table 3 Included angles between the protein major axis $\vec{X}_I'$ (of native or unfolded cyt *c* with the denaturants indicated) and the helical vectors, $\vec{\alpha}_N$, $\vec{\alpha}_C$, and $\vec{\alpha}_{60}$, the heme ligand vectors $\vec{v}_{Fe-S(Met80)}$ and $\vec{v}_{Fe-Trp59}$, and the total dipole moment $\vec{v}_D$ (*cf.* Fig. 5)

	Native (°)	Acid pH 1.9 (°)	8 M Urea (°)	4 M GuHCl (°)
$\vec{\alpha}_N$	119	119	131	140
$\vec{\alpha}_C$	99	98	79	83
$\vec{\alpha}_{60}$	88	88	107	113
$\vec{v}_{Fe-S(Met80)}$	65	64	50	58
$\vec{v}_{Fe-Trp59}$	74	73	87	96
$\vec{v}_D$	94	93	73	68

unfolded cyt *c* superimposed onto the native structure indicates the elongation orientation of the native protein during the unfolding.

As illustrated in Fig. 6, the native and unfolded protein structures are aligned by overlapping the common transition dipole moment $\vec{\mu}_e$ (proved to be stable during the unfolding processes previously). An unfolding trend is illustrated by the reorientation of the protein major axis, from $\vec{X}_N'$ to $\vec{X}_U'$, with respect to the intrinsic emission transition dipole moment of Trp59. Note that the helices of the native cyt *c* move with the green and blue loops during unfolding towards the ellipsoidal conformation of the dotted zone. The hence aligned protein morphologies suggest the trends of relocation of the local structures (vectors), from the native to the unfolded envelope morphology. For instance, N-terminal and C-terminal alpha-helices

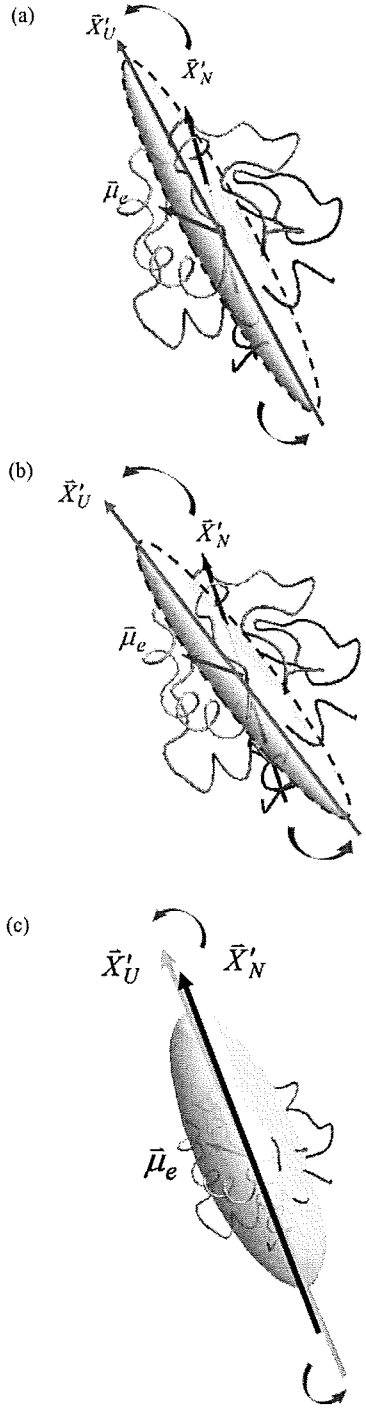

Fig. 6 The overlapped native (wireframe) and unfolded (shaped ellipsoidal region) conformations of the protein, based on the common emission transition dipole moment $\vec{\mu}_e$ (red arrow) of Trp59. The unfolded protein envelopes and the projected major axes are cyt *c* in the respective denaturants of (a) 4 M GuHCl; (b) 8 M urea; and (c) acid pH 1.9. The black and gray arrows stand for the major axes of $\vec{X}_N'$ and $\vec{X}_U'$, respectively.

and the loop structures of the globular native protein need to squeeze into the substantially elongated ellipsoidal envelope of the unfolded protein with urea as shown in Fig. 6. Also the unfolded cyt *c* in GuHCl follows a similar unfolding trend. In contrast, there are

This journal is © the Owner Societies 2016

relatively smaller relocations of these vectors in acid unfolding, as there are only marginal reorientations of the protein major axis (*cf.* Tables 1 and 3).

We have also deduced the included angles for $\vec{v}_{Fe-S(Met80)}$ and $\vec{v}_{Fe-Trp59}$ of the native protein and the cyt *c* unfolded with acid and the GuHCl denaturant. The results (Table 3) suggest that Met80 and Trp59 may slide significantly away from the heme group (Fig. 5b) in the urea and GuHCl unfolding. This would suggest breaking of the ligand bond of Fe–Met80, which was indeed observed previously with X-ray absorption spectroscopy (XAS) for the urea-unfolding.[45] Our molecular dynamics simulation for cyt *c* with 8 M urea (detailed in S12, ESI†) also suggests consistently that without breaking the heme ligands of Fe–Met80 and Fe–His18, the protein could not unfold at all to the large aspect ratio observed with SAXS (*cf.* Fig. 2).[46]

3.5 Environment-dependent unfolding behaviors

Fig. 5 and 6 summarize our TRFA–SAXS results, suggesting that cyt *c* unfolds *via* developing an elongated orientation $\vec{X}_U'$. Accompanied are the different extents of relocations of the terminal α helices and loop structures of the protein in the corresponding unfolding pathways. Previous studies,[19,20] however, suggested that acid- and denaturant-induced unfolding sequences of cyt *c* were similar. In our previous studies,[30,31] we showed that the unfolding sequence and the free energies extracted for the urea-induced unfolding of cyt *c* were consistent with that proposed in the literature.[19,20] Nevertheless, our previous[30,31] and current TRFA–SAXS results suggest consistently that the unfolding behaviour of cyt *c* in pH titration is somewhat different, based on the correlated global and local conformational changes observed. The different opinions on the acid-induced unfolding behaviour of cyt *c* may be attributed to the selected probes of respective structural sensitivities. As suggested in our previous SAXS measurements for global conformational changes in acid-induced unfolding,[31] the protein surface charge effect of the acid-unfolded cyt *c* might lead to a rearrangement of hydrogen bonds in the protein unfolding for a relatively less elongation of the hence unfolded protein structure. Whereas NMR reveals the structural changes of local specific residues of the protein in terms of their proton exchange, and the sensitivity could be stringent in an environment rich in protons for acid-induced protein unfolding.

Our previous studies[30,31] based on a modified Ising model suggested that cytochrome *c* adopts specific stepwise unfolding sequences with five structure groups (G^0–G^5), depending on denaturing environments. The groups G^1 and G^2 are correlated to the local protein structures near heme; the G^3 group is associated with the helical secondary structure, and G^0 and G^4 are responsible for the global structural change of the protein. The pH-sensitive group G^0, having f_u = 1/2 at pH = 5.7, behaves similarly to that of the 40–57 Ω-loops of the protein reported previously.[20] Compared with the sequence of the folding proposed by Hu *et al.*[19] and Krishna *et al.*[20] the G^1 group might correspond to 71–85 Ω-loops, responsible for breaking the bond of Fe–Met80, and is half-unfolded (with the unfolding fraction f_u = 1/2) at 5.7 M urea and a pH value of 3.1.[20,30,31] Our previous work proposed that cyt *c* follows the unfolding sequence of $G^0 \rightarrow G^1 \rightarrow G^4 \rightarrow G^2 \rightarrow G^3$ in acid-induced unfolding; which differs from the sequence $G^1 \rightarrow G^2 \rightarrow G^3 \rightarrow G^4$ observed in urea-induced unfolding.[31]

We also notice that the global conformation of the unfolded cyt *c* in the denaturing environments with pH = 1.9 is close to that partially unfolded in 6.5 M urea.[31] Nevertheless, the corresponding circular dichroism (CD) spectra suggested a much more dissociated secondary structure of the protein at pH = 1.9, also implying different unfolding pathways. Moreover, non-negligible coupling energy of cyt *c* was only found in the acid-induced unfolding process, but not in urea- or GuHCl-induced unfolding process.[31] All these differences observed suggest that different responses of the unfolded protein to different denaturing environments may lead to different protein unfolding pathways.

With 5.1 M GuHCl, drastic changes in the dynamic structure of CO stretching mode of the heme of cyt *c* was observed by 2D-IR spectroscopy,[27,28] and referred to as a glassy state of unfolded cyt *c*. Our TFRA–SAXS results also suggest relatively compact forms with an ellipsoid-like shape for the unfolded conformations of cyt *c*, which are clearly different from the globular shape of the native protein or a random-coil-like assembly of amino acids characterized by a power-law SAXS behaviour of $I(q) \propto q^{-2}$ (Fig. 2). Moreover, the delicate unfolded protein envelopes extracted based on GASBOR further suggest that the unfolded protein conformations have richer surface features (or ruggedness) than the native one. These morphological features may be relevant to the features of the glassy-like state, involving hydrophobic collapse, of unfolded cyt *c* suggested previously by Kim *et al.*, based on the site-specific vibrational probe of 2D-IR.[27] Moreover, the stepwise unfolding sequence explained by our modified Ising model suggests that the unfolded cyt *c* could be refolded in thermodynamics, following the hierarchical folding model.[47] If the protein obeys the reversible folding–unfolding sequences, the revealed cyt *c* refolding sequences will agree with the hydrophobic collapse folding model. The hydrophobic collapse model of protein folding–unfolding, however, may be better examined with time-resolved SAXS in μs time resolution for the folding–unfolding kinetics and the re-folding process of the protein.

4. Conclusions

With integrated SAXS and TRFA, we have used an intrinsic coordination in describing the global and local structural changes of cytochrome in different denaturing environments. The characteristic unfolding pathway of cytochrome *c* under stimulation of urea, GuHCl, or acid could be differentiated *via* reorientation of the major axis of the protein morphology (regarded as a preferred unfolding direction) with respect to the stable emission transition dipole moment of Trp59 of the protein. Changes in the relative positions of the terminal alpha-helices and loop structures of cytochrome *c* to the protein major axis in the unfolding are revealed based on the proposed

protein internal coordination. The joint SAXS–TRFA study, together with intrinsic coordination proposed here, provides a novel method in revealing correlated global and local structural changes in folding–unfolding of proteins with appropriate fluorophores. For further validation with unfolded proteins, the proposed methodology could be tested with, such as pH-dependent or temperature dependent protein unfolding.

Acknowledgements

The authors thank very much Prof. C. Y. Mou of National Taiwan University and Prof. A. C. Su of National Tsing-Hua University for helpful suggestions and discussions. This work was supported by MOST 103-2113-M-002-011 and Academia Sinica.

References

1 J. R. Winkler and H. B. Gray, *Chem. Rev.*, 2014, **114**, 3369.
2 T. Otosu, K. Ishii and T. Tahara, *Nat. Commun.*, 2015, **6**, 7685.
3 R. L. Baldwin and G. D. Rose, *Curr. Opin. Struct. Biol.*, 2013, **23**, 4.
4 B. Schuler and H. Hofmann, *Curr. Opin. Struct. Biol.*, 2013, **23**, 36.
5 D. Thirumalai, Z. Liu, E. P. O'Brien and G. Reddy, *Curr. Opin. Struct. Biol.*, 2013, **23**, 22.
6 S.-H. Chen, L. Liu, E. Fratini, P. Baglioni, A. Faraone and E. Mamontov, *Proc. Natl. Acad. Sci. U. S. A.*, 2006, **103**, 9012.
7 D. Matsuoka, S. Sugiyama, M. Murata and M. Nakasako, *J. Phys. Chem. B*, 2015, **119**, 114.
8 S. Khodadadi, J. H. Roh, A. Kisliuk, E. Mamontov, M. Tyagi, S. A. Woodson, R. M. Briber and A. P. Sokolov, *Biophys. J.*, 2010, **98**, 1321.
9 D. Nonaka, H. Wariishi, K. G. Welinder and H. Fujii, *Biochemistry*, 2010, **49**, 49.
10 S. Casalini, G. Battistuzzi, M. Borsari, C. A. Bortolotti, G. Di Rocco, A. Ranieri and M. Sola, *J. Phys. Chem. B*, 2010, **114**, 1698.
11 S. Hirota, Y. Fujimoto, J. Choi, N. Baden, N. Katagiri, M. Akiyama, R. Hulsker, M. Ubbink, T. Okajima, T. Takabe, N. Funasaki, Y. Watanabe and M. Terazima, *J. Am. Chem. Soc.*, 2006, **128**, 7551.
12 J.-R. Huang, F. Gabel, M. R. Jensen, S. Grzesiek and M. Blackledge, *J. Am. Chem. Soc.*, 2012, **134**, 4429.
13 S. Fiedler, J. Broecker and S. Keller, *Cell. Mol. Life Sci.*, 2010, **67**, 1779.
14 J. R. Grigera and A. N. McCarthy, *Biophys. J.*, 2010, **98**, 1626.
15 A. Hagarman, L. Duitch and R. Schweitzer-Stenner, *Biochemistry*, 2008, **47**, 9667.
16 C. H. Henkels and T. G. Oas, *J. Am. Chem. Soc.*, 2006, **128**, 7772.
17 Y.-Y. Cheng, S. H. Lin and H.-C. Chang, *J. Phys. Chem. A*, 2003, **107**, 10687.
18 J. R. Huang, L. R. Warner, C. Sanchez, F. Gabel, T. Madl, C. D. Mackereth, M. Sattler and M. Blackledge, *J. Am. Chem. Soc.*, 2014, **136**, 7068.
19 W. Hu, B. T. Walters, Z.-Y. Kan, L. Mayne, L. E. Rosen, S. Marqusee and S. W. Englander, *Proc. Natl. Acad. Sci. U. S. A.*, 2013, **110**, 7684.
20 M. M. G. Krishna, H. Maity, J. N. Rumbley, Y. Lin and S. W. Englander, *J. Mol. Biol.*, 2006, **359**, 1410.
21 T. Cellmer, E. R. Henry, J. Hofrichter and W. A. Eaton, *Proc. Natl. Acad. Sci. U. S. A.*, 2008, **105**, 18320.
22 M. B. Prigozhin and M. Gruebele, *Phys. Chem. Chem. Phys.*, 2013, **15**, 3372.
23 M.-T. Lee, T.-L. Sun, W.-C. Hung and H. W. Huang, *Proc. Natl. Acad. Sci. U. S. A.*, 2013, **110**, 14243.
24 L. Fu, Z. Wang and E. C. Y. Yan, *Int. J. Mol. Sci.*, 2011, **12**, 9404.
25 T. Weidner and D. G. Castner, *Phys. Chem. Chem. Phys.*, 2013, **15**, 12516.
26 B. Ding, A. Panahi, J.-J. Ho, J. E. Laaser, C. L. Brooks III, M. T. Zanni and Z. Chen, *J. Am. Chem. Soc.*, 2015, **137**, 10190.
27 S. Kim, J. K. Chung, K. Kwak, S. E. J. Bowman, K. L. Bren, B. Bagchi and M. D. Fayer, *J. Phys. Chem. B*, 2008, **112**, 10054.
28 J. K. Chung, M. C. Thielges and M. D. Fayer, *Proc. Natl. Acad. Sci. U. S. A.*, 2011, **108**, 3578.
29 U. Jeng, C.-H. Hsu, Y.-S. Sun, Y.-H. Lai, W.-T. Chung, H.-S. Sheu, H.-Y. Lee, Y.-F. Song, K.-S. Liang and T.-L. Lin, *Macromol. Res.*, 2005, **13**, 506; U. Jeng, C.-H. Hsu, H.-S. Sheu, H.-Y. Inigo, A. R. Lee, H. C. Chiu, W. S. Fann, S. H. Chen, A. C. Su, T.-L. Lin, K. Y. Peng and S. A. Chen, *Macromolecules*, 2005, **38**, 6566.
30 Y.-J. Shiu, U.-S. Jeng, C. Su, Y.-S. Huang, M. Hayashi, K.-K. Liang, Y.-L. Yeh and S.-H. Lin, *J. Appl. Crystallogr.*, 2007, **40**, s195.
31 Y.-J. Shiu, U.-S. Jeng, Y.-S. Huang, Y.-H. Lai, H.-F. Lu, C.-T. Liang, I.-J. Hsu, C.-H. Su, C. Su, I. Chao, A.-C. Su and S.-H. Lin, *Biophys. J.*, 2008, **94**, 4828.
32 G. W. Bushnell, G. V. Louie and G. D. Brayer, *J. Mol. Biol.*, 1990, **214**, 585.
33 U. Jeng, C. H. Su, C.-J. Su, K.-F. Liao, W.-T. Chuang, Y.-H. Lai, J.-W. Chang, Y.-J. Chen, Y.-S. Huang, M.-T. Lee, K.-L. Yu, D.-G. Liu, C.-F. Chang, C.-Y. Liu, C.-H. Chang and K. S. Liang, *J. Appl. Crystallogr.*, 2010, **43**, 110.
34 Y.-S. Huang, U.-S. Jeng, Y.-J. Shiu, Y.-H. Lai and Y.-S. Sun, *J. Appl. Crystallogr.*, 2007, **40**, s165.
35 D. I. Svergun, M. V. Petoukhov and M. H. J. Koch, *Biophys. J.*, 2001, **80**, 2946.
36 R. G. Gordon, *J. Chem. Phys.*, 1966, **45**, 1643.
37 L. D. Favro, *Phys. Rev.*, 1960, **119**, 53.
38 T. Tao, *Biopolymers*, 1969, **8**, 609.
39 A. Szabo, *J. Chem. Phys.*, 1980, **72**, 4620.
40 A. J. Ruggiero, D. C. Todd and G. R. Fleming, *J. Am. Chem. Soc.*, 1990, **112**, 1003.
41 G. R. Fleming, *The international series of monographs on chemistry: Chemical application of ultrafast spectroscopy*, Oxford university press, New York, 1986, pp. 124–134.

 This journal is © the Owner Societies 2016

42 M. Li, Y.-S. Huang, U.-S. Jeng, I.-J. Hsu, Y. C. S. Wu, Y.-H. Lai, C.-H. Su, J.-F. Lee, Y. Wang and C.-C. Chang, *Biophys. J.*, 2009, **97**, 609.
43 D. Zhong, S. K. Pal, D. Zhang, S. I. Chan and A. H. Zewail, *Proc. Natl. Acad. Sci. U. S. A.*, 2002, **99**, 13.
44 E. J. Stollar, J. L. Gelpi, S. Velankar, A. Golovin, M. Orozco and B. F. Luisi, *Proteins: Struct., Funct., Bioinf.*, 2004, **57**, 1.
45 I.-J. Hsu, Y.-J. Shiu, U.-S. Jeng, T.-H. Chen, Y.-S. Huang, Y.-H. Lai, L.-N. Tsai, L.-Y. Jang, J.-F. Lee, L.-J. Lin, S.-H. Lin and Y. Wang, *J. Phys. Chem. A*, 2007, **111**, 9286.
46 D. A. Case, T. E. Cheatham III, T. Darden, H. Gohlke, R. Luo, K. M. Merz Jr., A. Onufriev, C. Simmerling, B. Wang and R. J. Woods, *J. Comput. Chem.*, 2005, **26**, 1668.
47 S.-R. Yeh and D. L. Rousseau, *Nat. Struct. Biol.*, 2000, **7**, 443.